High Contrast Imaging with NGST and the Detection of Nearby Planetary Systems

John T. Trauger

Jet Propulsion Laboratory, California Institute of Technology, Pasadena, CA 91109

Abstract. A coronagraphic camera provides NGST with unique discovery capabilities. Enabled science programs and the corresponding instrument concept, as recently developed in the context of an NGST ISIM study, are summarized here.

1. Introduction

The scientific case for NGST is an inevitable outgrowth of the stunning success of the Hubble Space Telescope (HST). HST is the first space observatory to exploit the imaging characteristics available to a diffraction-limited space observatory at visible wavelengths. NGST will extend this discovery space to include diffraction-limited imaging at infrared wavelengths.

A coronagraph camera module (CCM) provides access to phenomena within the nearest few arcseconds of bright stars and quasars. CCM broadens NGST's reach to include the complex environments of the nearest stars and the engines that power AGN in distant galaxies. Science programs enabled by an NGST coronagraph include a representative survey of nearby planetary systems, substellar companions, and reflection nebulae associated with embryonic and evolved stars in our galactic neighborhood – a class of objects that would otherwise be lost in the glare of the central star. The corresponding prerequisites for instrument and telescope design have been evaluated in terms of high-fidelity computer modelling.

The following report summarizes an ISIM concept study of high-contrast Origins science (HCOS) strategies for NGST. The HCOS study explored a number of potential science programs (Trauger *et al.* 1999) as summarized in Section 2. Engineering concepts for a coronagraph have been extended somewhat beyond the HCOS report, as discussed in Section 3. Finally, a non-coronagraphic camera mode with smooth pupil apodization for improved contrast in crowded fields of stars is considered in Section 4.

2. Science Program

Five broad scientific objectives have been identified. These include the nature of mature planets and brown dwarf companions in the solar neighborhood; the protoplanetary disks, gaseous jets, and very young planets still radiating their accretion energy associated with young stellar objects; the properties of tenuous

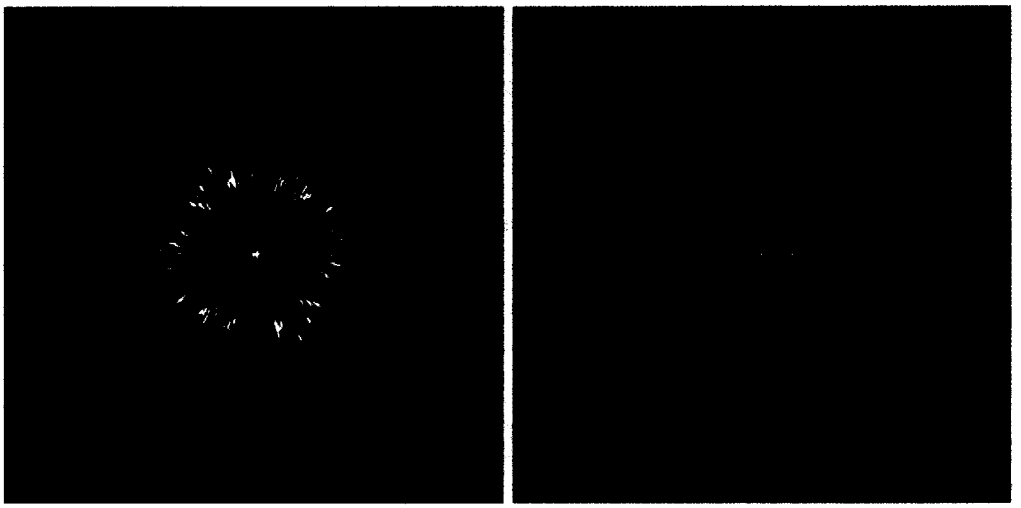

Figure 1. *Simulated NGST/CCM image of Lalande 21185 (a main-sequence M2 dwarf at 2.5 pc) with an assumed jovian planet separated by 5AU, taken in a single M band exposure of 0.5 hours. A large brightness enhancement beyond blackbody is predicted for methane-blanketed giant planets and brown dwarfs at M (Burrows* et al. *1997). The detectibility of younger and/or more massive companions is even more favorable than the case for 5GY jupiters. At left is the direct detection with HST-quality primary mirror surface finish. At right, the NGST surface finish is assumed to scatter ten times that of the HST, and a reference PSF star has been subtracted.*

exozodiacal debris disks in more evolved planetary systems; and the processes by which evolved stars expel their harvest of heavy elements into the galactic medium, the raw material for the next generation of stars and planets. Beyond our galactic neighborhood, the coronagraph also offers unique discovery potential in bright quasar environments.

2.1. Extra-Solar Giant Planets and Brown Dwarf Companions

A central scientific objective for NGST/CCM is the direct detection of jovian planets orbiting stars in the solar neighborhood. Direct imaging provides photometric information that is not available from astrometric and radial velocity measurements. Direct photometry is needed to characterize the luminosity, temperature, and atmospheric structure of these objects, and to place them in context with the planets of our solar system. Direct imaging has the added advantage that it is no more difficult to detect complex systems with multiple planets than a single planetary companion. It provides the means to further investigate many planetary systems discovered in groundbased radial velocity searches, including the recent discovery of three EPGs around υ Andromedae (Butler *et al.* 1999) and others that will inevitably be discovered in the next several years.

The HCOS study identified the spectrum near 5μm as an especially attractive lever for the study of jovian planets and brown dwarfs. At this wavelength, atmospheres with $T_{eff} < 1200$K are significantly cleared of molecular opacity, allowing thermal emission from warmer, deeper levels of the objects to escape directly to space. Jupiter's disk shows broad "hot spots" in 5μm images (Ortiz *et al.* 1998). The spectrum of GL229B also shows a prominent flux enhancement at 5μm (Oppenheimer *et al.* 1998). Theoretical spectra from model brown dwarf atmospheres consistently show the same bright emission near 5μm, and indicate that these objects can be many orders of magnitude brighter than an equivalent blackbody radiator at the planet's effective temperature (Burrows *et al.* 1997; Allard *et al.* 1996). For example, the 5μm contrast between a Jupiter-like companion and an M star primary (such as Lalande 21185) is 6×10^6. The superthermal emission of EGPs and BDs at 5μm offers a distinct opportunity for NGST planet detection.

Direct EGP detections are possible in single short exposures if the NGST optics match the HST in surface figure, as in Figure 1 (at left). For the HCOS survey, however, it was assumed that the scatter from the optical surfaces would exceed HST by a factor of ten, and that each image would be processed by subtracting the image of a reference star, as shown in Figure 1 (at right). The effects of scattering and diffraction in the instrument are combined with backgrounds from solar system zodiacal emission and emission from the telescope primary to estimate the background level against which a planet must be detected. Shot noise on this background and detector noise are combined to estimate integration times for planet detection at $S/N = 10$. Exposure times are calculated for actual Gliese catalog objects, using their apparent magnitudes and distances (Gliese and Jahreiss, 1979). This is a somewhat conservative detection criterion, since planets will always appear as point-like images whereas residual speckles take on a spectrally dispersed and streaked appearance in broad-band images. Additional image processing with spatial filtering could provide better sensitivity, but is not assumed in our feasibility criterion.

CCM can provide a nearly complete search for giant planet companions in a sample of nearby single stars (d < 10 pc), aimed at detecting EGPs at least as bright as Jupiter (i.e. mass = 0.001 $M_\odot$, age = 4.5 Gyr, absolute M magnitude 23) at separations of 5 AU. Using a 10% bandwidth M filter, the survey will be able to detect Jupiters around *all* single stars within 8 pc in integration times of 3 hours or less, and around a significant fraction of other stars at greater distances. Detection of more luminous (more massive and/or younger) or more widely separated companions will be correspondingly easier, and can be accomplished for progressively more distant systems from the Sun. A total of 90 targets are available within 8 pc.

Further, CCM can search for brown dwarf companions in a sample of nearby single stars (d < 20 pc), targeting BDs/EGPs brighter than an absolute M magnitude of 19. Since the brightnesses of BDs/EGPs depend on both their masses and their ages, each observed magnitude defines a curve in the mass-age plane. For reference, either a young 1 M_J object at $\sim$ 1Gyr or a more massive 5 M_J object at $\sim$ 5 Gyr would have an absolute M magnitude of 19. Using relatively short integration times (< 0.5 hr/object), NGST can expect to obtain

a nearly complete census of BD/EGP companions among a sample of about 500 stars.

For the brightest objects uncovered in these surveys, the coronagraph can carry out spectrophotometric observations with filters and grisms covering λ=1-5μm. In summary, an observational program using an NGST coronagraphic camera can be expected to provide the first determination of the giant planet/brown dwarf luminosity function and the first spectral characterization of these objects across a broad range of effective temperatures. In conjunction with mass determinations for the companions from astrometric surveys, photometric measurements with CCM will allow the theoretical cooling curves for substellar objects to be compared with actual luminosity and temperature measurements. Finally, an NGST coronagraph can produce the first direct images of planets orbiting other stars. Such an investigation, using capabilities that are unique to NGST, is of fundamental scientific importance to our understanding of planetary systems and their frequency in nature.

2.2. Young Stellar Objects

Our planetary system is believed to have formed from a flattened cloud of gas and dust which orbited the Sun very early in its history. Infrared and millimeter wavelength spectroscopic studies indicate that 50% of young stars possess circumstellar disks with masses and sizes comparable to our formative planetary system (Beckwith *et al.* 1990). Protoplanetary disks in the nearest star-forming regions have outer radii of only a few arcseconds, and their surface brightnesses in reflected light (in mag/arcsec^2) are at least 10 mag fainter than the central point source. Several of these objects have now been imaged optically by HST in special circumstances of external illumination (McCaughrean and O'Dell 1996) or edge-on orientation (Burrows *et al.* 1996; Stapelfeldt *et al.* 1998), and imaged in the near-infrared using adaptive optics in a few cases (Roddier *et al.* 1996). However, HST and adaptive optics imaging have failed to detect disks in scattered light around the majority of young stars studied thus far, even though millimeter maps and infrared photometry already indicate that resolvable disks are present in the systems (McCaughrean *et al.* 1999).

A NGST coronagraph can reveal the structure of protoplanetary disks at radii corresponding to our Solar System's Kuiper Belt. At the distance of the nearest star-forming clouds, NGST provides a spatial resolution of 5 AU at 2μm wavelength. CCM observations can provide direct measurements of disk outer radii and radial brightness profiles. Multicolor imaging will allow a disk's dust properties to be diagnosed, and comparison of the images with scattered light models will allow a disk's scale height and density profile to be derived. These data will lead to a better understanding of the physical conditions in the outer parts of the protoplanetary disk, the formation region of cometary planetesimals. In the more face-on disks, NGST/CCM images will reveal radial structures in the disk mass distribution. These may include inner holes or gaps dynamically induced by stellar or planetary companions, and wakes, density waves, or accretion streams in binary systems. The coronagraph will enable direct imaging of young jovian planets themselves within the disk. A 5 M_J object at age 10 million years presents a contrast of 10^{-5} versus a central T

Tauri star. NGST/CCM can detect all such objects in the nearest star-forming clouds at projected separations of 30 AU or larger.

Coronagraphic NIR imaging with NGST will track the dispersal of proto-planetary disks, and help to establish the timescales for the settling of dust to the disk mid-plane, the depletion of dust as the grains coagulate into planetesimals, and the final clearing of the initial dust inventory from the system.

2.3. Debris Disks and Structures

About 15% of main sequence stars are known to possess circumstellar dust to the sensitivity limits of the IRAS survey (Backman and Paresce 1993). These debris disks span four orders of magnitude in dust density, from the tenuous zodiacal light in our own solar system to the disk of β-Pictoris. In all these systems, the survival timescale for an individual dust grain against Poynting-Robertson drag is relatively short, only 10^6 to 10^7 years. The presence of such short-lived material around stars long after their original protoplanetary disks have dispersed requires the ongoing production of new dust particles by processes such as collisions within planetesimal populations (comets and asteroids) and sublimation of comets during periastron passages. Further, shattering collisions and star-grazing orbits imply the presence of planetary-mass perturbers. The mere existence of main sequence debris disks is indirect evidence for the presence of planets.

An NGST coronagraph will resolve the internal structures of debris disks in reflected light. In comparison to the recent HST/NICMOS results for HR 4796 at 2μm (Schneider *et al.* 1999), NGST will allow higher resolution imaging studies of systems more than an order of magnitude more tenuous. Direct imaging of extrasolar zodi and KB dust structures at high spatial resolution and in numerous distant systems will allow the disks' radial extents, density profiles, central clearings, edges, and major asymmetries to be resolved, providing compelling indirect evidence for planets in such systems. To date, only the two densest debris disks (β-Pic and HR 4796) have been detectable in scattered light at the low contrast levels which have been accessible at near-IR wavelengths. The β-Pic disk contains asymmetries most easily explained as due to the dynamical influence of planets, including a mid-plane warp that could be caused by a jovian mass with orbit inclined to the disk grains and their parent bodies (Burrows *et al.* 1995). Such morphological features provide indirect evidence of embedded planets. Optical simulations indicate that Kuiper debris disk systems with dust optical depths of a few times 10^{-5} (similar to that of Fomalhaut, or a few hundred times that of the Zodiacal cloud) will be accessible to NGST/CCM in a few hours of integration time. Initial estimates from IRAS detection statistics imply that hundreds of such targets with spectral types A-K are available within 60 pc of the Sun.

2.4. Near-Environment of AGB and Post-AGB Stars

The mass-loss processes that accompany late stellar evolution are responsible for the enrichment of the ISM with the products of nucleosynthesis. The circumstellar envelopes of dying stars contain the key to understanding the mass ejection which generate proto-planetary and planetary nebulae (PPNe and PNe). All stars in the 1-8 $M_\odot$ mass range eject half or more of their initial mass during

the last few 10^4 years of AGB evolution and produce PNe. More massive stars also lose mass at comparable rates during a supergiant phase just before ending their lives as Type II supernovae. The ejection of material is accompanied by the creation the PNe structures, probably through the interaction of fast collimated stellar winds with ambient circumstellar material in the NSE.

Yet, the process of mass-loss in these objects remains very poorly understood because the near-stellar environment (NSE) within about 100 stellar radii (one stellar radius extends ~2-4 AU) contains structures that are typically orders of magnitude fainter than the glare of the bright central star. Dust-scattered stellar continuum radiation and the spectral lines of neutral and ionized gas from these the NSE will be accessible to an NGST coronagraph. An NGST coronagrph will resolve the region of stellar wind acceleration (20-200 R_*) in several hundred AGB red giants/supergiants within 100-1000 pc and provide a representative sampling of the ubiquitous mass-loss phenomenon. NSE morphologies – symmetric or asymmetric, smooth or clumpy, continuous or episodic – will provide important new constraints for models of mass loss phenomena.

2.5. QSO Origins and Host Galaxies

The remarkable commonality between the history of QSOs and the star formation rate in the universe suggests that common physical mechanisms govern the formation and evolution of QSOs and their host galaxies. Do QSOs form as a natural consequence of mergers or starburst activity in the cores of protogalaxies? Is there a threshold for the local density of protogalaxies which must be met to trigger the formation of massive black holes? What did galaxies look like as they formed the earliest QSOs? To answer these questions, we must travel back to a time when both QSOs and galaxies are forming, redshifts greater than ~2, and compare the environments we see with NGST to those detected around low redshift objects.

There is evidence at low and moderate redshifts (with some theoretical and numerical support) that galaxy mergers and interactions are largely responsible for the fueling of AGN activity. Such phenomena should be more frequent and more spectacular during the early stages of galaxy formation and evolution, and in particular near the peak merging epoch, believed to be around the redshifts of 2 to 3 (see e.g., Baugh *et al.* 1998). It is probably not a coincidence that the comoving density of quasars peaks at the same redshifts (Hartwick and Schade 1990). Yet, at present there is practically nothing known about the host galaxies and immediate environments of quasars at such redshifts. This is a purely observational limitation, since the light of the QSOs greatly outshine their host galaxies and close companions. A coronagraphic camera is a natural solution.

Adequate imaging of QSO hosts and environments at very modest redshifts (a few tenths) can be already accomplished with the HST using simple imaging and PSF subtraction techniques (Bahcall *et al.* 1997). The NGST coronagraph makes it possible to extend such observations to the peak of the QSO era, to $z \sim 2-3$. In addition, even for low and moderate redshifts, CCM imaging of QSO hosts would reveal structures such as small-scale bars and circumnuclear starbursts, at smaller separations from the nucleus than is possible with the simple PSF subtraction alone.

3. Coronagraph Concept for NGST

A coronagraphic camera is among several strategies that have been considered for high-contrast imaging in future space astronomy missions. Other approaches that have been reported recently include various combinations of interferometric deep nulling, multi-aperture telescope arrays, active wavefront correction, aggressive pupil apodization, and dark speckle processing (Angel and Woolf 1997; Beichman *et al.* 1999; Moutou *et al.*1998; Rabbia *et al.* 1998; Woolf and Angel 1998). With its large filled aperture, the NGST provides an ideal setting for high contrast coronagraphic imaging.

3.1. NGST Telescope Architecture

As part of the integrated science instrument module (ISIM), the coronagraphic camera is designed for compatibility with the NGST telescope architecture. The NGST architecture is still a work in progress, hence the design approach makes use of the available knowledge of the "yardstick" NGST and a sensitivity analysis for those system characteristics that are as yet undefined or unknown. The yardstick NGST projects a jitter-stabilized f/24 optical beam to a focal plane shared by all instruments in the ISIM. The optical wavefront is corrected to a nominal $\lambda/14$ rms (diffraction limited) at 2 microns wavelength. Telescope pointing is stabilized to 0.0027 arcseconds rms by one or more fine steering mirrors (FSMs). The ISIM shrouds and structural members will be passively cooled to 35 Kelvins.

However, all high-contrast imaging strategies will be sensitive to scatter from residual mirror surface figure errors and diffraction from the mirror segmentation geometry, both of which are not sufficiently defined by the yardstick NGST. Performance of a coronagraph is fundamentally limited by speckle – the faint, noisy haze of light caused by coherent scatter from low-amplitude irregularities on telescope optical surfaces. The NGST has baselined an active mirror correction of its optical wavefront, either as an actuated primary mirror or further along the optical path as a small deformable mirror. It will thereby suppress speckle to a maximum angular separation from the central star that corresponds to the density of actuators on the corrective mirror, creating a "dark hole" in the focal plane (Malbet, Yu, and Shao 1995). It is in this dark hole that NGST will provide its highest contrast imaging.

Coronagraph concepts favor a primary mirror with a small number of large segments over other designs. This is because each additional mirror edge introduces its own diffraction, surface figure rolloff, and wavefront phase discontinuities that must be masked in the coronagraph optics. A seven-hexagon segmented primary mirror configuration, specifically a TRW design for NGST with 9m aperture edge-to-edge, is assumed here. Other proposed segmentation schemes have also been modeled. In general those telescopes designed with a few large segments give nearly identical coronagraphic science performance, and the seven-hexagon architecture is representative of any of these large-segment designs.

3.2. Optical Design

A coronagraph is defined by two essential elements – an occulting mask in the focal plane to reject the light from a bright central point source, and a Lyot stop at a subsequent pupil plane to remove the light that has bypassed the occulting mask due to diffraction by the telescope structures and mirror edges.

Simulations have shown that both high-contrast coronagraphy (using the occulting spot and Lyot stop) and improved crowded field performance (using only a smoothly graded Lyot stop) can be incorporated into an otherwise generic three-mirror NIR camera. For reference, an optical design for the coronagraphic camera has been developed in CodeV that includes three spherical mirrors in a near-Oeffner configuration plus a flat pickoff mirror. The pickoff mirror intercepts the NGST focal plane far enough upstream to bring the NGST image within the camera structure, where a fixed occulting spot is placed. A Lyot stop is provided by a multiple filter wheel mechanism placed at a well-defined pupil image halfway between the second and third mirrors of the three-mirror camera. The removable Lyot stop (or stops) allows the camera to revert to a normal unapodized imaging mode when desired.

CCM uses an apodized or graded-density occulting mask at the first focal plane, with transmittance shaped to the gaussian form $\tau = 1 - exp[-(r/\sigma)^2]$, where r is radial distance from the center of the occulting spot. Because the mask is partially transmitting and smoothly graded, the coronagraph imaging extends essentially to the center of the mask. This form of occulting spot concentrates the diffracted light near the perimeter of the pupil, where it is effectively removed by the Lyot mask. The optimal diameter for the occulting mask is wavelength dependent. CCM therefore includes occulting masks designed for best performance at the two primary science wavelengths of 2μm and 4.5μm. These are located in the focal plane of the telescope. Telescope pointing is used to place the central object on the appropriate occulting spot.

The Lyot mask can be a simple element machined from a thin metal disk. The dimensions of the Lyot mask depend on the shape and optical characteristics of the telescope primary mirror and support structures. For this study, the Lyot geometry transmits the central 80% of the segment dimensions of the outer six hexagons, resulting in an overall attenuation of approximately 50% of the incident light at the Lyot stop.

A selection of optical filters (R$\sim$5-10) and grisms (R$\sim$100) facilitates imaging and low resolution photometry/spectroscopy as required by the proposed science program. Large format InSb and HgCdTe detector arrays currently under development are expected to meet NGST's NIR performance requirements over the 0.8-5μm spectrum. The f/18 coronagraph camera, working with a detector 2048^2 array of 18μm pixels, provides a plate scale of $0.026''$/pixel and critical sampling at 2μm wavelength. With an expected dark rate of 0.03 electrons/pixel/sec and a read noise of order 3 electrons while sampling up the ramp, the detector background will remain below the zodiacal background limit for proposed HCOS science programs over the entire 0.8-5μm spectral range.

3.3. Science Performance Models

Traditional measures of low-order surface errors, including rms surface roughness and Strehl ratio, are not by themselves a sufficient metric for coronagraph

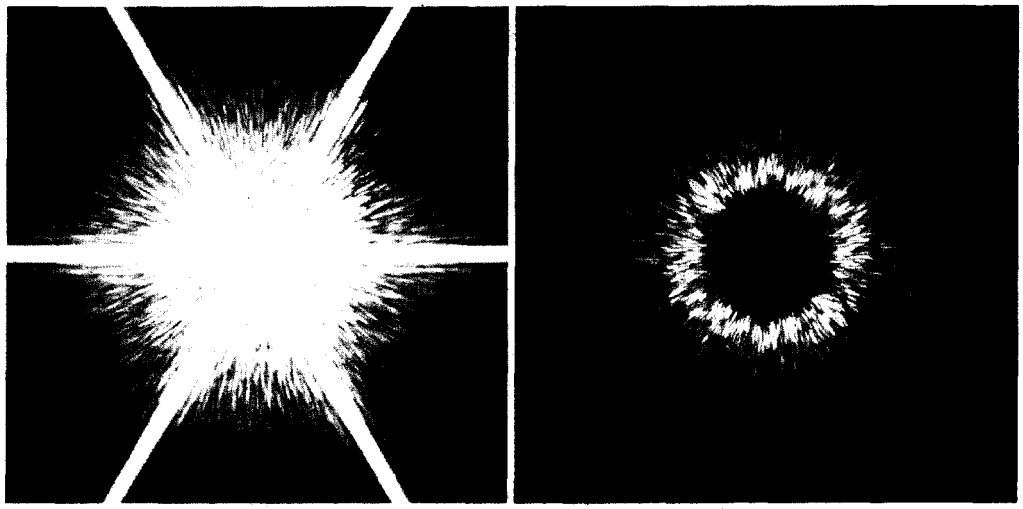

Figure 2. *At left is the point spread function (PSF) computed for NGST with a 10% bandwidth filter at 4.95μm wavelength, including a seven-hexagon primary mirror with predicted levels of mirror misalignment and surface figure errors. At right is the result of adding a coronagraph occulting spot and Lyot mask, showing that the bright central peak has been replaced by a high contrast "dark hole". Both images cover a 25 arcecond square field of view.*

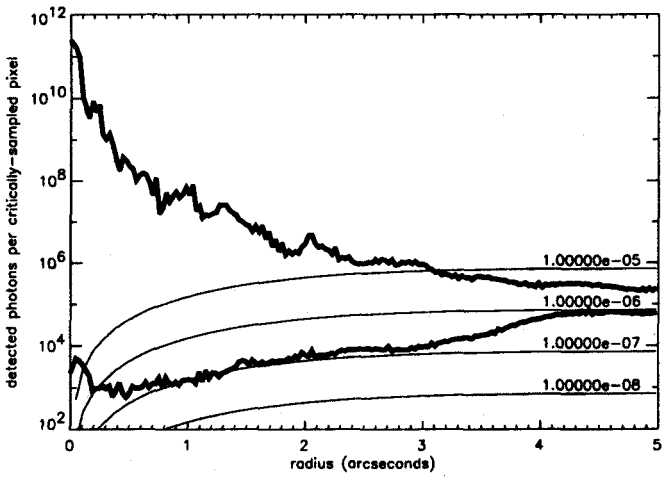

Figure 3. *Median flux per critically sampled pixel versus radius for the nominal NGST (upper curve) and with the addition of the coronagraph (lower curve). These data correspond to the 4.95μm PSF images in Figure 2.*

performance. In fact, the coronagraph performance is largely insensitive to small amounts of focus and low-order surface distortions because these errors affect mainly the core of the point spread function (PSF). Surface figure errors with spatial frequencies in the range of $\sim 0.005 - 0.05$ cycles/cm will scatter starlight into the nearest few arcseconds from the star. Control of surface figure errors in this spatial-frequency range are critical to the unique CCM science program.

Instead, we note that in the smooth-surface limit, the angular distribution of the light scattered from a mirror surface maps the power spectral density

(PSD) of its residual surface roughness (Church *et al.* 1979). We have obtained estimates of the PSD from a number of large-aperture high quality aspheric mirrors, including the HST primary mirror (after correction of its low order spherical aberration), and find that their PSD versus spatial frequency typically follows a power law at spatial frequencies greater than a few$\times$0.01 cycles/centimeter. We have adopted a "yardstick" surface figure metric by fitting a curve of the form PSD $= A/[1 + (\kappa/\kappa_0)^n]$ to the azimuthally averaged surface PSD derived from the HST phase map (e.g. Krist and Burrows 1995). We use this form to define an isotropic PSD approximation to the HST surface figure, with n = 3, $A = 5.8 \times 10^5 A^2 cm^2$, and $\kappa_0 = 0.03 cycles/cm$. This PSD metric can be translated into an encircled energy specification for the NGST telescope optical system. Each of seven individual mirror segments is assigned surface figure errors that conform to PSDs scaled from the HST "yardstick".

The optical model includes a simulation of the on-orbit optical alignment procedure for the deployed NGST primary mirror. The seven randomly misaligned hexagonal mirror segments are brought into alignment and co-phased using a star image. Next, phase retrieval techniques are used estimate residual mirror figure errors. A modified Gerchberg-Saxton iteration is used, simultaneously operating on a pair of defocussed images (Redding *et al.* 1998). This procedure avoids the need for dedicated wavefront sensing instrumentation while providing a true end-to-end measure of the NGST/ISIM optical train. Figure correction on each of the seven primary mirror segments is carried out with up to 394 actuators working on each, according to the Arizona mirror design concept (Angel and Burge 1999). The surface influence profile of the mirror actuators has been characterized in terms of a structural finite-element model constrained by laboratory measurements. Actuator positional errors are then introduced. The alignment procedure iterates until the diffraction limit is achieved at 2μm wavelength. No further wavefront corrections are assumed.

The NGST/CCM model then simulates NGST imagery by including effects of detector pixel sampling, coronagraph occulting and Lyot masks, optical aberrations and tolerances, measured and generated mirror surface errors, pointing jitter, detector characteristics including read noise and dark background rates, zodiacal background, spectral bandwidth of the optical filters, and photon statistics for the target object.

It is this model that has been used to estimate the coronagraph science performance. NGST image characteristics are illustrated in Figure 2 (at left), a simulated NGST exposure of a single star at 4.95μm with a 10% bandwidth filter and a total detected signal of 10^{12} electrons. At right in Figure 2 is the same star, wavelength, and exposure time, but with the addition of the CCM coronagraphic masks. The Lyot mask accepts about 50% of the NGST pupil area. In both examples, the mid-frequency surface figure PSD on the primary mirror is ten times worse than the HST yardstick, and the mirror actuator positional errors correspond to a step size of 10 nm. Figure 3 indicates the contrast available to the coronagraph. The smooth curves superimposed on the data indicate the signal that would be obtained in the central pixel from a planet companion, at any given separation from the star, that is fainter than the central star by the indicated factors. This model, adjusted as appropriate for wavelength range, background, and exposure levels, has been used for the entire

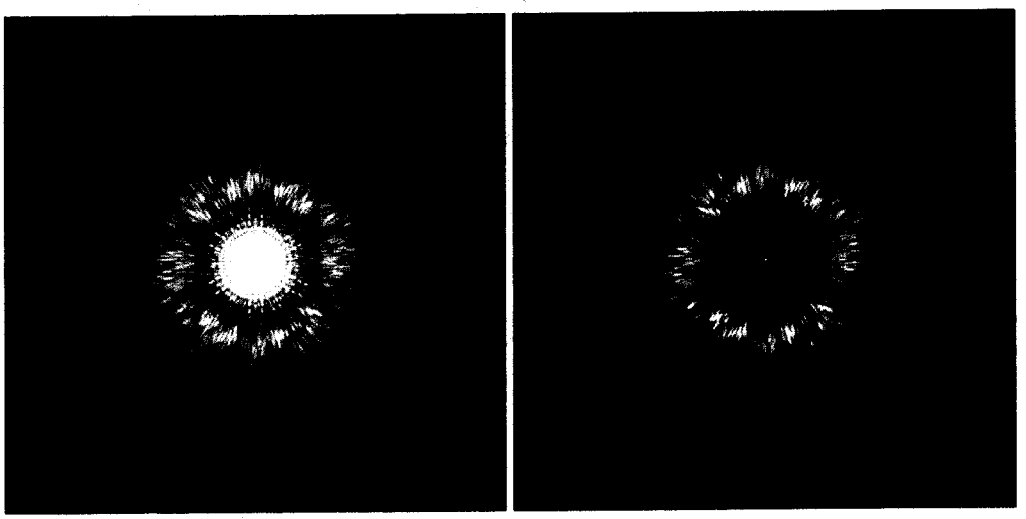

Figure 4. *Simulations of the NGST PSF at 4.95μm wavelength apodized with a sonine profile, with and without the coronagraph occulting spot. At left is a simulation that includes the expected levels of NGST mirror misalignment and surface figure errors. Shown at right is the result of adding a coronagraphic occulting spot; the bright central peak has been replaced by a high contrast "dark hole". Both images cover a 25" square field of view, and intensities are displayed with the same logarithmic contrast stretch as used in Figure 2.*

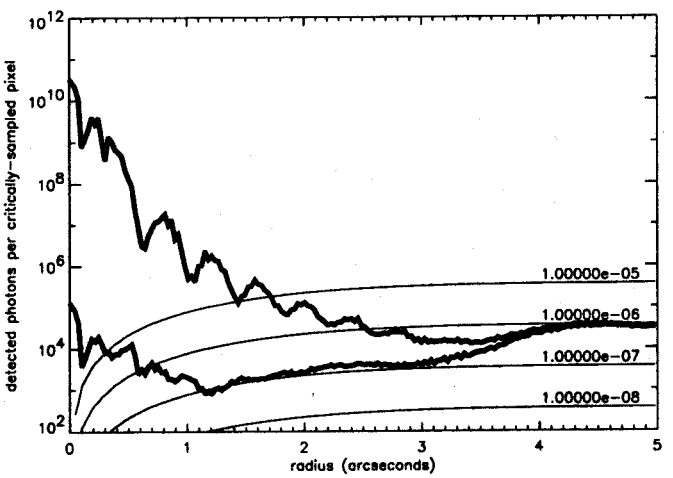

Figure 5. *Median flux per critically sampled pixel versus radius for the sonine-apodized NGST at 4.95μm wavelength (upper curve) and with the addition of a coronagraph occulting spot (lower curve). These data are taken from the 4.95μm PSF images in Figure 4.*

HCOS science program summarized in Section 2, with the single exception of the direct planet detection shown at left in Figure 1, which used a PSD matching the HST yardstick and an actuator step size of 3 nm.

4. Pupil Apodization for Crowded Fields

Access to large crowded fields is one of the unique advantages of space astronomy. In crowded fields of stars, significant sky background levels can accumulate from the extended light of numerous nearby stars. For reference, the energy from a star that falls beyond a radius of 0.6″for NGST at 2μm wavelength is predicted to be in the range of 4-8%, a number that will depend on the final specification for mid-frequency surface figure on the primary mirror. Smooth apodization of the NGST pupil is a strategy that can improve the contrast between crowded stars and background light by as much as two orders of magnitude. This is illustrated in Figure 4 (at left), where transmittance has been apodized by the form $S = [1 - (r/r_0)^2]$ applied to the outer six hexagonal segments, and r_0 is the radius of a circle inscribed within the individual hexagons. This pupil apodization transmits 25% of the light reaching the NGST primary. Figure 4 assumes the same star, wavelength, and exposure time as for Figure 2, and the image is displayed with the same logarithmic contrast stretch. The contrast improvement, which applies simultaneously to all stars within the field of view, can be seen in Figure 5. Also shown in Figure 4 (at right) is the result of blocking the light of a single isolated star with a coronagraphic occulting spot. Performance is comparable to the coronagraph in the previous section, but with the light collecting efficiency reduced by one half due to the more aggressive pupil mask. The option of pupil apodization can be implemented with a selectable masking element mounted in a filter wheel located within the NIR camera optics, making improved contrast available when required for crowded field programs that can accept a corresponding reduction in efficiency.

5. Conclusions

The optimal coronagraph for NGST is undoubtedly an instrument that takes full advantage of NGST's telescope architecture – an instrument that is fully "integrated" into its ISIM environment. The foregoing summary and the ISIM study report (Trauger *et al.* 1999) outline a simple NIR coronagraphic camera that provides unique and compelling science programs for NGST.

References

Allard, F., P.H. Hauschild, I. Baraffe, G. Chabrier 1996, ApJ, 465, L123

Angel, J.R. and J. Burge 1999, "Ultraviolet-Optical Space Astronomy Beyond HST," ASP Conference Series 164, J.M. Shull, A. Kinney, and J. Morse eds., 234

Angel, J.R. and N.J. Woolf 1997, ApJ, 475, 393

Backman, D.E., and F. Paresce 1993, in "Protostars and Planets III", E.H. Levy and J.I. Lunine eds, University of Arizona Press, Tucson, 1253

Bahcall, J.N., et al. 1997, ApJ, 386, L1

Baugh, C., S. Cole, C. Frenk, and C. Lacey 1998, ApJ, 498, 504

Beckwith, S., A.I. Sargent, R. Chini, and R. Gusten 1990, AJ, 99, 924

Beichman, C.A., N.J. Woolf, and C.A. Lindensmith (eds) 1999, "The Terrestrial Planet Finder (TPF)", JPL Publication 99-3

Burrows, A., M. Marley, W.B. Hubbard, J.I. Lunine, T. Guillot, D. Saumon, R. Freedman, D. Sudarsky, C. Sharp 1997, ApJ, 491, 856

Burrows, C.J. et al. 1995, BAAS, 187, 3205

Burrows, C.J. et al. 1996, ApJ, 473, 437

Butler, R.P., G.W. Marcy, D.A. Fischer, T.W. Brown, A.R. Contos, S.G. Korzennik, P. Nisenson, R.W. Noyes 1999, ApJ

Church, E.L., H.A. Jenkinson, and J.M. Zavada 1979, Opt Eng, 18, 125

Gliese, W., and H. Jahreiss 1979, Astron. Astrophys. Suppl. 38, 423

Hartwick, F.D.A., and D. Schade 1990, ARA&A, 28, 437

Krist, J., and C.J. Burrows 1995, Applied Optics, 34, 4951

Malbet, F., J. Yu, and M. Shao 1995, PASP 109, 386

McCaughrean, M.J., K.R. Stapelfeldt, and L. Close 1999 in Protostars and Planets IV, V. Mannings, A. Boss, and S. Russell eds., Univ. of Arizona Press, Tucson, in press

McCaughrean, M.J. & C.R. O'Dell 1996, AJ, 111, 1977

Moutou, C., A. Boccaletti, and A. Labeyrie 1998, Proceedings of the 34th Liege Colloquium (ESA SP-429), 211

Oppenheimer, B., S.R. Kulkarni, K. Matthews, M.H. van Kerkwijk 1998, ApJ, 502, 932

Oritz, J.L., G.S. Orton, A.J. Friedson, S.T. Stewart, B.M. Fisher, J.R. Spencer 1998, JGR, 103, 23051

Rabbia, Y., P. Baudoz, and J. Gay 1998, Proceedings of the 34th Liege Colloquium (ESA SP-429), 279

Redding, D., S. Basinger, A. Lowman, A. Kissil, P. Bely, R. Burg, G. Mosier, M. Femiano, M. Wilson, D. Jacobson, J. Rakoczy, J. Hadaway 1998, SPIE paper, 3356-47, Kona HI

Roddier, F., C. Roddier, M.J. Northcott, J.E. Graves, and K. Jim 1996, ApJ, 463, 326

Schneider, G., B.A. Smith, E.E. Becklin, D.W. Koerner, R. Meier, D.C. Hines, P.J. Lowrance, R.J. Terrile, R.I. Thompson, M. Rieke 1999, ApJ, 513, L127

Stapelfeldt, K.R. et al. 1998, ApJ, 502, L65

Trauger, J., K. Stapelfeldt, R. Sahai, D. Backman, C. Beichman, G. Djorgovski, M. Ealey, E. Gaidos, C. Grillmair, Y. Gursel, S. Kulkarni, R. Lyon, S. Macenka, C. Martin, M. Ressler, M. Shao, and M. Werner 1999, "High Contrast Origins Science for NGST", NGST ISIM Concept Study Report, http://ngst.gsfc.nasa.gov/public_docs.html

Woolf, N.J. and J.R. Angel 1998, ARA&A, 36, 507